

Regularization by Texts for Latent Diffusion Inverse Solvers

Jeongsol Kim^{1,*}, Geon Yeong Park^{1,*}, Hyungjin Chung¹, and Jong Chul Ye²

¹ Dept. of Bio & Brain Engineering, KAIST

² Kim Jae Chul AI graduate school, KAIST

{jeongsol, pky3436, hj.chung, jong.ye}@kaist.ac.kr

* Equal contribution

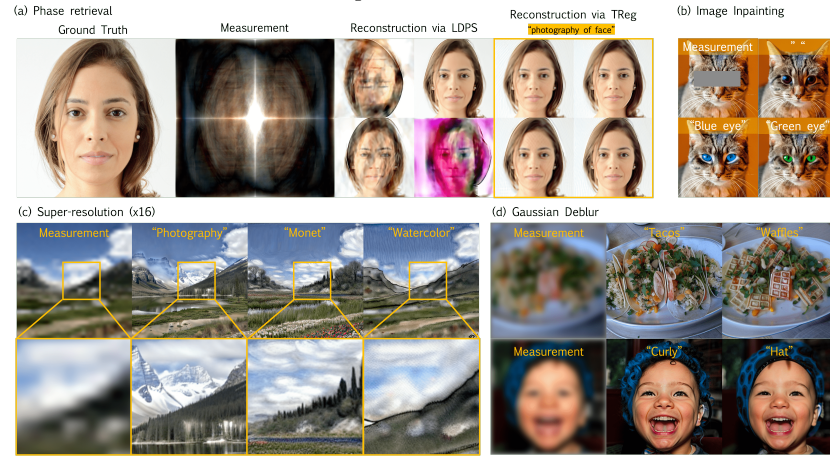


Fig. 1: (a) TReg breaks inherent system symmetry in the phase retrieval problem, leading to consistent solutions for multiple trials. Additional results by TReg for (b) image inpainting, (c) super-resolution (x16), and (d) Gaussian deblurring task with text-driven regularization. Note that images are reconstructed according to the given text prompt while preserving the data consistency with the given measurement.

Abstract. The recent advent of diffusion models has led to significant progress in solving inverse problems, leveraging these models as effective generative priors. Nonetheless, there remain challenges related to the ill-posed nature of such problems, often due to inherent ambiguities in measurements or intrinsic system symmetries. To address this, drawing inspiration from the human ability to resolve visual ambiguities through perceptual biases, here we introduce a novel latent diffusion inverse solver by *regularization by texts* (TReg). Specifically, TReg applies the textual description of the preconception of the solution during the reverse diffusion sampling, of which the description is dynamically reinforced through null-text optimization for adaptive negation. Our comprehensive experimental results demonstrate that TReg successfully mitigates ambiguity in the inverse problems, enhancing their effectiveness and accuracy.

Keywords: Inverse problems · Text regularization · Latent diffusion model

1 Introduction

Consider a given forward measurement process:

$$\mathbf{y} = \mathcal{A}(\mathbf{x}) + \epsilon \quad (1)$$

where $\mathcal{A} : \mathbb{R}^m \mapsto \mathbb{R}^n$ describes imaging systems, $\mathbf{y} \in \mathbb{R}^n$ and $\mathbf{x} \in \mathbb{R}^m$ represents the measurement and the true image, respectively, and $\epsilon \in \mathbb{R}^n$ denotes the measurement noise. Then, an inverse solver attempts to recover \mathbf{x} from the measurement \mathbf{y} .

Unfortunately, the majority of the inverse problems are ill-posed, implying that many different visual inputs produce the same measurements as a significant amount of visual information in the original input is lost during the measurement process. For example, Fourier phase retrieval, a problem of reconstructing the phase information of a signal from only its Fourier intensity measurements, is a notorious example of an ill-posed inverse problem due to the intrinsic system symmetries such as shift, rotation, and flips. So when inverting such systems, an input is mapped to multiple symmetry-related outputs.

Classically, regularization techniques have been extensively studied to address the ambiguity in inverse problems. For example, sparsity (L_1 norm), total variation (TV), and regularization by denoising (RED) have been widely used for regularization by exploiting the statistical properties of natural images [4,27,37]. With the advent of the diffusion model, a new family of Diffusion Inverse Solvers (DIS) [7,18,25,38] have been proposed with superior reconstruction performance. The main idea is to leverage the power of the diffusion model that has learned the score function of prior distribution to reduce the ill-posedness of the inverse problem.

While diffusion models have enabled substantial progress in inverse problems, it is important to note the persistent disparity between human perception and DIS. For example, in Fourier phase retrieval, Diffusion Posterior Sampling (DPS) [7,30] can recover the true signal much better than traditional approaches, but they are still not able to completely break the intrinsic symmetry as illustrated in Figure 1(a). This is because the diffusion prior is based on image statistics, and image statistics alone might not be sufficient to break the symmetry and ensure a unique solution. In contrast, the human visual system easily distinguishes whether the obtained solution is semantically meaningful or not. This ability likely stems from perceptual biases obtained through our experience with natural scenes, particularly in tasks like facial recognition. In fact, perceptual bias plays a crucial role in how we perceive and understand the world around us, especially in situations where visual information is incomplete, ambiguous, or open to multiple interpretations. However, no equivalent mechanism in DIS currently applies these preconceptions during reconstruction.

To bridge the gap between human perception and diffusion inverse solvers (DIS), here we introduce a new concept, *Regularization by Text (TReg)*, by utilizing latent diffusion models. TReg specifically employs textual descriptions reflecting the preconceived notion of the desired outcome during the reverse

sampling phase. However, a straightforward application of a text prompt reflecting these preconceptions is inadequate, as the intermediate images from reverse samples vary in noise levels. To effectively integrate the textual form of the preconception and guide the reverse sampling, we therefore propose an innovative adaptive negation method by null text optimization throughout the reverse diffusion sampling process. This approach dynamically adjusts the influence of the textual guide, ensuring it aligns with the evolving state of the reverse sampling. For example, TReg with regularization prompt of "photography of face" can break the symmetry in Fourier phase retrieval and consistently obtains a unique true solution, as shown in Figure 1(a). Moreover, our method is so general that it can be applied for any inverse problem in a zero-shot manner, by reducing the uncertainty and improving accuracy, as shown in 512x512 images in Figure 1 (b-c).

2 Background

2.1 Latent diffusion model

Image diffusion models that operate on the pixel space are compute-heavy. So the latent diffusion model (LDM) [28] is a class of diffusion-based generative models [16, 31, 35], where the diffusion process is operated on low dimensional latent space instead of the pixel space. Specifically, the LDMs are trained as a variational autoencoder by maximizing the evidence lower bound (ELBO) [19, 28]. Thus, the latent is represented as:

$$\mathbf{z} = \mathcal{E}_\phi(\mathbf{x}) := \mathcal{E}_\phi^\mu(\mathbf{x}) + \mathcal{E}_\phi^\sigma(\mathbf{x}) \odot \boldsymbol{\epsilon}, \quad \boldsymbol{\epsilon} \sim \mathcal{N}(0, \mathbf{I}), \quad (2)$$

where \odot denotes the element-by-element multiplication, and $\mathcal{E}_\phi^\mu, \mathcal{E}_\phi^\sigma$ are parts of the encoder that outputs the mean and the variance of the encoder distribution. The resulting pixel domain representation can be obtained by

$$\mathbf{x} = \mathcal{D}_\varphi(\mathbf{z}) \quad (3)$$

where \mathcal{D}_φ is the decoder.

Then, the forward diffusion starts from the latent representation for the clean image $\mathbf{z}_0 = \mathcal{E}(\mathbf{x}) \in \mathbb{R}^d$ and generates samples $\mathbf{z}_t = \sqrt{\bar{\alpha}_t}\mathbf{z}_0 + \sqrt{1 - \bar{\alpha}_t}\boldsymbol{\epsilon}$ using VP-SDE formulation. Accordingly, the neural backbone $\boldsymbol{\epsilon}_\theta(\cdot, t)$ is trained to estimate the noise $\boldsymbol{\epsilon}$ from \mathbf{z}_t by solving the following optimization problem:

$$\min_{\theta} \mathbb{E}_{\mathcal{E}_\phi(\mathbf{x}), \boldsymbol{\epsilon} \sim \mathcal{N}(0, \mathbf{I}), t} [\|\boldsymbol{\epsilon} - \boldsymbol{\epsilon}_\theta(\mathbf{z}_t, t)\|_2^2], \quad (4)$$

where the neural network $\boldsymbol{\epsilon}_\theta$ is commonly selected as time-conditional UNet [29]. Notably, the optimal solution $\boldsymbol{\epsilon}_\theta^*$ of (4) can be used to derive a score function as $\nabla_{\mathbf{z}_t} \log p(\mathbf{z}_t) = -\boldsymbol{\epsilon}_\theta^*(\mathbf{z}_t, t)/\sqrt{1 - \bar{\alpha}_t}$ [35]. After training, we can conduct the reverse sampling from the posterior distribution $p_\theta(\mathbf{z}_{t-1}|\mathbf{z}_t, \mathbf{z}_0)$ as

$$\hat{\mathbf{z}}_{0|t} = \mathbb{E}[\mathbf{z}_0|\mathbf{z}_t] = (\mathbf{z}_t - \sqrt{\bar{\alpha}_t}\boldsymbol{\epsilon}_\theta(\mathbf{z}_t, t))/\sqrt{\bar{\alpha}_t} \quad (5)$$

$$\mathbf{z}_{t-1} = \sqrt{\bar{\alpha}_{t-1}}\hat{\mathbf{z}}_{0|t} + \sqrt{1 - \bar{\alpha}_{t-1}}\boldsymbol{\epsilon}_\theta(\mathbf{z}_t, t), \quad (6)$$

under the assumption of deterministic DDIM sampling [33].

2.2 Classifier Free Guidance

By inheriting the classifier guidance of generative models, [13] proposed the classifier guidance for deterministic DDIM sampling by defining epsilon prediction that corresponds to $\nabla_{\mathbf{z}_t} \log p(\mathbf{z}_t|\mathbf{c})$,

$$\hat{\epsilon}_\theta(\mathbf{z}_t, \mathbf{c}, t) = \epsilon_\theta(\mathbf{z}_t, t) - \omega\sqrt{1 - \bar{\alpha}_t}\nabla_{\mathbf{z}_t} \log p(\mathbf{c}|\mathbf{z}_t) \quad (7)$$

where ω is a scale ³ for the guidance and $\nabla_{\mathbf{z}_t} \log p(\mathbf{c}|\mathbf{z}_t)$ is computed by a trained classifier. To reduce additional computation costs from classifier training, [17] proposed the classifier-free-guidance by substituting $\nabla_{\mathbf{z}_t} \log p(\mathbf{c}|\mathbf{z}_t) = \nabla_{\mathbf{z}_t} \log p(\mathbf{z}_t|\mathbf{c}) - \nabla_{\mathbf{z}_t} \log p(\mathbf{z}_t)$ so that the epsilon prediction is defined as

$$\hat{\epsilon}_\theta^\omega(\mathbf{z}_t, \mathbf{c}, t) = \epsilon_\theta(\mathbf{z}, \emptyset, t) + \omega(\epsilon_\theta(\mathbf{z}, \mathbf{c}, t) - \epsilon_\theta(\mathbf{z}, \emptyset, t)), \quad (8)$$

where \emptyset denotes *null-text* that indicates the class identifier for unconditional score prediction (i.e. $\epsilon_\theta(\mathbf{z}_t, t) = \epsilon_\theta(\mathbf{z}_t, \emptyset, t)$) to achieve both unconditional and conditional score prediction with a single neural network. It is noteworthy that the null-text token is also a learnable parameter of LDM.

2.3 Diffusion Inverse Solvers

Recently diffusion models have been extensively used as powerful generative priors for inverse problems [7, 8, 18, 25, 34, 38]. Earlier techniques in inverse imaging relied on an alternating projection method [5, 10, 35], enforcing hard measurement constraints between denoising steps in either pixel or measurement spaces. More advanced strategies have been proposed to approximate the gradient of the log posterior within diffusion models, broadening the scope to tackle nonlinear problems [7]. The field has seen further expansion with methods addressing blind inverse problem [6], 3D [9, 20], and problems of unlimited resolution [2].

Traditionally, these methods have utilized image-domain diffusion models, but a shift has been observed towards latent diffusion models such as latent DPS (LDPS) with a fixed point of autoencoder process [30], LDPS with history update [14] and Resample [32]. Despite these innovations, the use of text embedding for regularization is often overlooked, which we opt to address.

3 Main Contribution: Regularization by Text

In this section, we explain the details of TReg. Specifically, the reverse diffusion sampling by TReg consists of three distinct steps: 1) adaptive negation for reinforcing the textual constraint, 2) latent optimization to impose measurement and latent space consistency, and 3) forward process to return the intermediate reconstruction to correct noisy manifold. It is noteworthy that TReg is a zero-shot algorithm for general inverse problems without additional training or fine-tuning. The details are as follows.

³ If $\omega = 1.0$, $\hat{\epsilon}_\theta(\mathbf{z}_t, \mathbf{c}, t) = \sqrt{1 - \bar{\alpha}_t}\nabla_{\mathbf{z}_t} \log p(\mathbf{z}_t|\mathbf{c})$. Otherwise, we are approximating $p(\mathbf{z}_t|\mathbf{c}) \propto p(\mathbf{z}_t|\mathbf{c})p(\mathbf{c}|\mathbf{z}_t)^\omega$

3.1 Adaptive negation for textual constraint

While the text prompt for LDM can effectively narrow down the solution space, directly employing text prompts via CFG may not adequately capture the intended guidance due to the inherent error-prone nature of hand-crafted prompts. In other words, the provided text prompts may not represent optimal conditioning. To resolve this, one can leverage the prompt tuning [21], but it can disrupt the user intention included in the text prompt during the tuning process. Instead of finding an optimal text prompt that matches the user’s intention, we found that the concept negation [17] that comprises complement concepts of the given text prompt is effective in reinforcing the original user’s concept.

In particular, during the reverse sampling, we minimize the following cost function on the CLIP [26] embedding space:

$$\mathcal{L}_\theta = \text{sim}(\mathcal{T}_{img}(\hat{\mathbf{x}}_0(\mathbf{y})), \mathbf{c}_\theta), \quad (9)$$

where c_θ is the embedded null-text token via CLIP text encoder, \mathcal{T}_{img} denotes CLIP image encoder, $\hat{\mathbf{x}}_0(\mathbf{y})$ denotes denoised estimates on pixel space which is updated by the data consistency, and $\text{sim}(\cdot, \cdot)$ denotes inner product. By minimizing the similarity between intermediate images $\hat{\mathbf{x}}_0(\mathbf{y})$ and the null-text in the CLIP space, we can make the null-text have complementary concepts for given contexts which are accumulated to the intermediate images $\hat{\mathbf{x}}_0$. Specifically, leveraging the null-text token facilitates the concept negation and the suppression of the complement concept is achievable by optimizing the null-text token. This approach considers only the null-text token as a variable, and since back-propagation to other neural networks does not occur, the computational cost is negligible. This makes the proposed method extremely cost-effective for enhancing text guidance. Figure 2 (b) demonstrates that the adaptive negation significantly improves the reconstruction quality.

3.2 Latent Optimization

For the latent optimization, consider the following loss, which is the maximum a posteriori (MAP) objective under the VAE prior in (2) by assuming that $\mathcal{E}_\phi^\sigma(\mathbf{x})$ is isotropic, i.e. $\mathcal{E}_\phi^\sigma(\mathbf{x}) = \sigma_\varepsilon \mathbf{1}$:

$$\mathcal{L}(\mathbf{x}, \mathbf{z}) = \frac{\|\mathbf{y} - \mathcal{A}(\mathcal{D}_\varphi(\mathbf{z}))\|_2^2}{2\sigma^2} + \frac{\|\mathbf{z} - \mathcal{E}_\phi^\mu(\mathbf{x})\|_2^2}{2\sigma_\varepsilon^2}. \quad (10)$$

We can now minimize (10) using the proximal optimization. Specifically, for an initial latent $\mathbf{z}_0 := \hat{\mathbf{z}}_{0|t}$ from the Tweedie’s formula, the proximal approach compute the solution that minimizes the following:

$$\mathcal{L}(\mathbf{x}, \mathbf{z}) + \gamma \|\mathbf{z} - \hat{\mathbf{z}}_{0|t}\|^2 \quad (11)$$

which we are interested in solving by variable splitting similar in spirit to the alternating direction method of multipliers [4]. Namely, using the decoder approximation and setting $\mathbf{x} = \mathcal{D}_\varphi^\mu(\mathbf{z})$, the optimization problem with respect to

\mathbf{x} becomes

$$\min_{\mathbf{x}} \frac{\|\mathbf{y} - \mathcal{A}(\mathbf{x})\|_2^2}{2\sigma^2} + \frac{\|\mathbf{z} - \mathcal{E}_\phi^\mu(\mathbf{x})\|_2^2}{2\sigma_\xi^2} + \lambda \|\mathbf{x} - \mathcal{D}_\varphi(\mathbf{z}) + \boldsymbol{\eta}\|_2^2. \quad (12)$$

Here, for simplicity, we set dual variable $\boldsymbol{\eta}$ as a zero vector and do not consider its update. Then, from the initialization with $\mathbf{z} = \hat{\mathbf{z}}_{0|t}$, we have

$$\hat{\mathbf{x}}_0(\mathbf{y}) = \arg \min_{\mathbf{x}} \frac{\|\mathbf{y} - \mathcal{A}(\mathbf{x})\|_2^2}{2\sigma^2} + \lambda \|\mathbf{x} - \mathcal{D}_\varphi(\hat{\mathbf{z}}_{0|t})\|_2^2, \quad (13)$$

which can be solved with negligible computation cost such as conjugate gradient (CG). Subsequently, using the encoder approximation and setting $\mathbf{z} = \mathcal{E}_\phi^\mu(\mathbf{x})$ with $\boldsymbol{\eta} = \mathbf{0}$, the optimization problem with respect to \mathbf{z} reads

$$\hat{\mathbf{z}}_0^{ema} = \arg \min_{\mathbf{z}} \zeta \|\mathbf{z} - \hat{\mathbf{z}}_0(\mathbf{y})\|_2^2 + \gamma \|\mathbf{z} - \hat{\mathbf{z}}_{0|t}\|_2^2 \quad (14)$$

with the initialization of $\hat{\mathbf{z}}_0(\mathbf{y}) := \mathcal{E}_\phi(\hat{\mathbf{x}}_0(\mathbf{y}))$, leading to a closed-form solution

$$\hat{\mathbf{z}}_0^{ema} = \bar{\alpha}_{t-1} \hat{\mathbf{z}}_0(\mathbf{y}) + (1 - \bar{\alpha}_{t-1}) \hat{\mathbf{z}}_{0|t} \quad (15)$$

where ζ, γ are chosen to satisfy $\bar{\alpha}_{t-1} = \zeta / (\zeta + \gamma)$. Finally, for the optimized latent $\hat{\mathbf{z}}_0^{ema}$, the update rule of the DDIM [33] at timestep t is given as follows

$$\mathbf{z}'_{t-1} = \sqrt{\bar{\alpha}_{t-1}} \hat{\mathbf{z}}_0^{ema} + \sqrt{1 - \bar{\alpha}_{t-1}} \tilde{\boldsymbol{\epsilon}}_t \quad (16)$$

where $\tilde{\boldsymbol{\epsilon}}_t$ denotes the total noise given by

$$\tilde{\boldsymbol{\epsilon}}_t := \frac{\sqrt{1 - \bar{\alpha}_{t-1} - \eta^2 \tilde{\beta}_t^2} \hat{\boldsymbol{\epsilon}}_\theta + \eta \tilde{\beta}_t \boldsymbol{\epsilon}}{\sqrt{1 - \bar{\alpha}_{t-1}}} \quad (17)$$

In (16), $\eta \in [0, 1]$ is a parameter controlling the stochasticity of the update rule: $\eta = 0.0$ leads to fully deterministic sampling, whereas $\eta = 1.0$ with $\tilde{\beta}_t = \sqrt{(1 - \bar{\alpha}_{t-1}) / (1 - \bar{\alpha}_t)} \sqrt{1 - \bar{\alpha}_t / \bar{\alpha}_{t-1}}$ recovers the ancestral sampling of DDPMs. Empirically, we find that $\eta \tilde{\beta}_t = \sqrt{\bar{\alpha}_{t-1}} \sqrt{1 - \bar{\alpha}_{t-1}}$ results in robust performance. In other words, the total noise is computed by $\tilde{\boldsymbol{\epsilon}}_t := \sqrt{1 - \bar{\alpha}_{t-1}} \hat{\boldsymbol{\epsilon}}_\theta + \sqrt{\bar{\alpha}_{t-1}} \boldsymbol{\epsilon}$. To sum up, the proposed algorithm is described as in Algorithm 1.

3.3 Latent DPS with updated null-text

In image inpainting and phase retrieval, we found that alternating latent DPS steps with the aforementioned latent optimization steps improves the data consistency. In this case, we set $\hat{\mathbf{z}}_{0|t}(\mathbf{e}_\emptyset)$ denotes the Tweedie's formula computed with the null text embedding. Then, we can obtain the standard LDPS gradient equipped with $\hat{\mathbf{c}}_\emptyset$, the optimized null text embedding at previous timestep:

$$\mathbf{z}_{t-1} = \mathbf{z}'_{t-1} - \rho_t \nabla_{\mathbf{z}_t} \|\mathcal{A}(\mathcal{D}_\varphi(\hat{\mathbf{z}}_{0|t}(\hat{\mathbf{c}}_\emptyset))) - \mathbf{y}\| \quad (18)$$

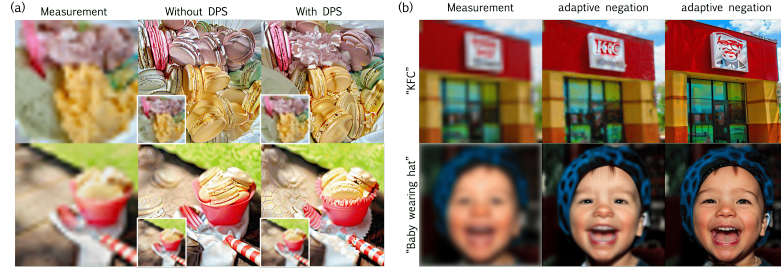
Algorithm 1 Inverse problem solving with TReg**Require:** $\epsilon_\theta, \emptyset, c, \mathcal{E}, \mathcal{D}, \mathcal{A}, y, \mathcal{T}_{img}$ $z_T \sim \mathcal{N}(0, \mathbf{I})$ **for** $t \in [T, 1]$ **do** $\hat{\epsilon}_\theta^\omega(z_t) = \epsilon_\theta(z_t, \emptyset, t) + \omega(\epsilon_\theta(z_t, c, t) - \epsilon_\theta(z_t, \emptyset, t))$ $\hat{z}_{0|t} = (z_t - \sqrt{1 - \bar{\alpha}_t} \hat{\epsilon}_\theta^\omega(z_t)) / \sqrt{\bar{\alpha}_t}$ $\tilde{\epsilon}_t \leftarrow$ Compute noise using (4)**if** $t \in \Gamma$ **then** $\hat{x}_0 \leftarrow \mathcal{D}(\hat{z}_{0|t})$ $\hat{x}_0(y) \leftarrow \arg \min_x \frac{\|y - \mathcal{A}(x)\|_2^2}{2\sigma^2} + \lambda \|x - \hat{x}_0\|_2^2$ $\hat{z}_0(y) \leftarrow \mathcal{E}(\hat{x}_0(y))$ $\hat{z}_0^{ema} \leftarrow \bar{\alpha}_{t-1} \hat{z}_0(y) + (1 - \bar{\alpha}_{t-1}) \hat{z}_{0|t}$ \triangleright Latent Optimization $z_{t-1} \leftarrow \sqrt{\bar{\alpha}_{t-1}} \hat{z}_0^{ema} + \sqrt{1 - \bar{\alpha}_{t-1}} \tilde{\epsilon}_t$ $c_\emptyset \leftarrow c_\emptyset - \eta \nabla_{\emptyset} \text{sim}(\mathcal{T}_{img}(\hat{x}_0(y)), c_\emptyset)$ \triangleright Adaptive negation**else** $z_{t-1} \leftarrow \sqrt{\bar{\alpha}_{t-1}} \hat{z}_{0|t} + \sqrt{1 - \bar{\alpha}_{t-1}} \tilde{\epsilon}_t$ **end if****end for**

Fig. 2: Ablation study on DPS update and adaptive negation. (a) Measurements are generated by SR (x16). Down-sampled images are displayed as insets. Class: "ice cream". Prompt "macaron". (b) Adaptive negation improves reconstruction.

where we set ρ_t to be the step size that weights the likelihood, similar to [7, 30]. On the other hand, in image super-resolution and deburring, we neglect the DPS update term for computational saving and just use Algorithm 1 as it is. Nevertheless, our algorithm can effectively solve the problem and shows comparable performance with DPS update as shown in Figure 2.

4 Experiments

The goal of text regularization is to refine the solution space by resolving ambiguity. Therefore, we evaluate two key aspects of the proposed method: 1) the effectiveness of TReg in resolving ambiguity, and 2) the accuracy of the obtained solution, which encompasses alignment with the text and measurements. For more details on experimental settings, refer to the Appendix.

4.1 Experimental settings

Forward models. We utilize extreme measurement conditions to demonstrate efficacy of our method. Specifically, we use the bicubic down-sampling with scale factor 16, Gaussian blurring with kernel size 61 and sigma 5.0. We define the linear forward operations and its transpose by following the previous studies [8, 18, 34, 38]. In the case of the box inpainting task, our intention is to employ a universal mask that encompasses the eyes and mouth of either animal or human. For this, we generate a box mask based on averaged images across all data points within each dataset. For Fourier phase retrieval, we obtain the Fourier magnitude by applying the Fourier transform to the image. In the formula, the forward model is expressed as $\mathbf{y} \sim \mathcal{N}(\mathbf{y}|FP\mathbf{x}_0, \sigma_0^2\mathbf{I})$, where F denotes the 2D Discrete Fourier Transform (DFT), P represents oversampling, that is implemented by adding 256 zero-padding to each side, and \mathbf{x}_0 denotes the clean image. For the measurement noise, the noise scale σ_0^2 is set to 0.01 for all tasks.

Baselines. The accuracy of the solution requires careful experimental design. As the first attempt to solve inverse problems using text-driven regularization, we establish baselines by combining 1) data consistency-preserving methods and 2) text-guided editing methods. Notably, these baselines involve sequential processing, while the proposed method stands out for its efficiency, eliminating the need for pre/post-hoc techniques. For data consistency methods, we utilize the measurement itself and PSLD [30] which is an LDM-based inverse problem solver. Regarding text-guided editing methods, we opt for state-of-the-art techniques, namely Delta Denoising Score (DDS) [15] and Plug-and-Play diffusion (PnP) [36]. Since PnP involves an inversion process, we handle it as a two-stage approach. Also, we use PSLD with text guidance as our baseline by applying CFG for computing the posterior mean. For the inpainting task, we utilize Stable-Inpaint, a fine-tuned stable diffusion model for the inpainting task, and Repaint [23] as our baseline. Finally, in the Fourier phase retrieval task, we compared the results with and without the text prompt using our framework to emphasize the effect of text guidance in breaking symmetry. In other words, for the baseline, we provided null text for the text condition.

Dataset and text prompt. For the effective quantitative evaluation of an obtained solution, it is crucial to select the measurement and text prompt that do not conflict with each other. This ensures that the generated features through textual guidance coherently maintain the data consistency across the entire dataset. Furthermore, selecting an improper text prompt \mathbf{c} (for instance, “dog” for the measurement generated by the baby image) can lead to undesired outcomes such as ignoring the provided guidance. After exploring various datasets, we have determined that the Food-101 dataset [3] is well-suited for our quantitative comparison due to its non-sparse and complex patterns. Also, given that all images in this dataset fall under the ‘food’ category, it becomes more straightforward to select an appropriate \mathbf{c} aligned with the original caption. Specifically, we leverage 250 images from each of the “fried rice” and “ice cream” classes, accompanied by the corresponding text prompts “spaghetti” and “macarons”. Also, we design the null-text update schedule since the reconstructed images become

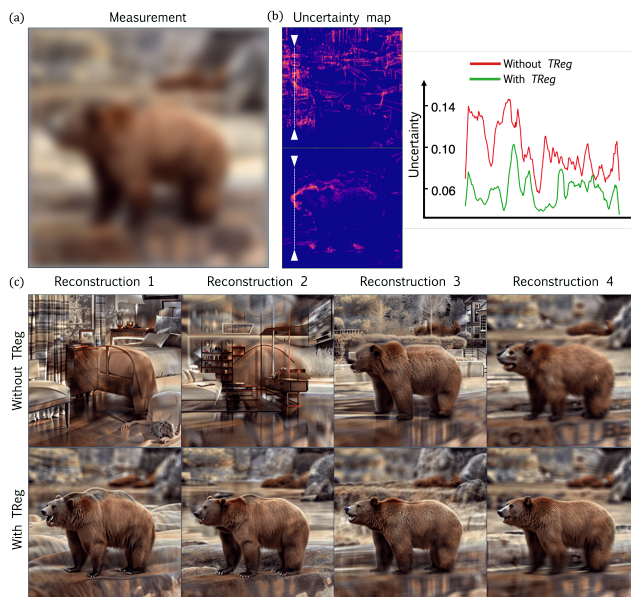


Fig. 3: TReg reduces the ambiguity. Given text prompt for TReg is "bear". (a) Measurement is generated by Gaussian blur. (b) Pixel-wise standard deviation is displayed. Uncertainty value across white dotted lines on measurement is plotted. Gaussian smoothing with a kernel width of 10 pixels is applied for visualization. (c) Reconstructed solutions from multiple trials.

saturated and fidelity is decreased if the null-text is optimized too frequently. Therefore, we apply updates to the null text only when data consistency updates are performed. For the optimization, we use AdamW [22] optimizer with learning rate $1e-3$ and update null-text for 10 iterations per time step. For the qualitative comparison, we additionally use a validation set of ImageNet [12]. For the inpainting, we select the AFHQ and FFHQ datasets for analysis to assess the efficiency of the proposed method across diverse domains. For the Fourier phase retrieval, we utilize the FFHQ dataset, since a general text prompt such as "photography of face" effectively describe the entire dataset and is adequate for resolving ambiguity arising from rotation or flip.

4.2 Experimental Results

Ambiguity reduction. To assess the capacity of TReg in reducing ill-posedness, we perform a comparative evaluation between the diffusion-based inverse solver with and without the TReg component. The elimination of TReg involves employing a null-text (\emptyset) as the text prompt while retaining adaptive negation, serving as an additional tool to suppress complementary concepts and enhance the generated image quality. We solve the inverse problem 10 times with different random seeds for a fixed super-resolution measurement.

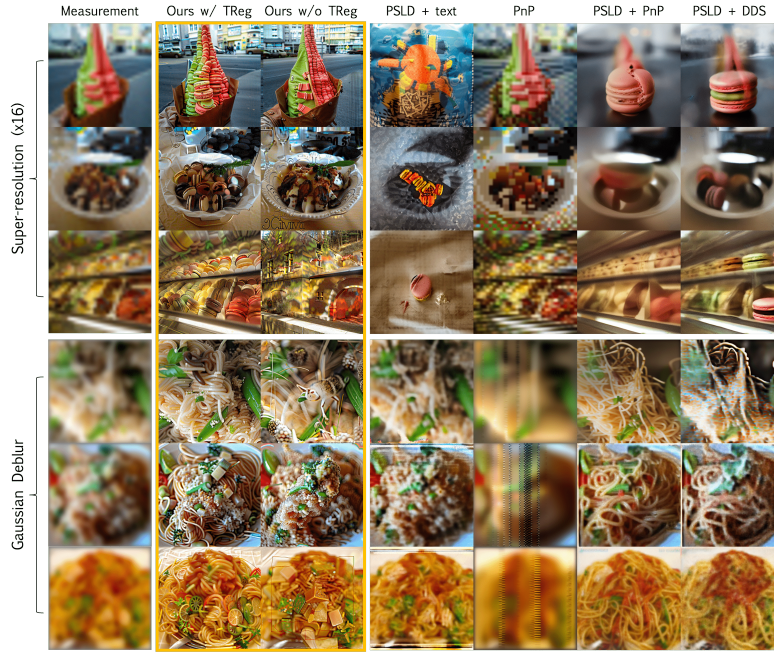


Fig. 4: Representative reconstructed images for super-resolution (x16) and Gaussian deblurring. SR: Original class is "ice cream" and given prompt is "macaron". Deblur: Original class is "fried rice" and given prompt is "spaghetti".

The result, depicted in Figure 3, demonstrates that the TReg leads to a unique solution corresponding to the given prompt. Conversely, in the absence of TReg, reconstructed images exhibit multiple solutions, such as a car in the background or a bedroom. This discrepancy is clearly observed in its uncertainty map in Figure 3 which is defined as pixel-wise standard deviation values, revealing heightened uncertainty levels without TReg, particularly in regions corresponding to distinct objects or characters. Although TReg implementation reduces uncertainty, some residual uncertainty persists, primarily attributed to in-class variations, notably in aspects like head positioning or mouth shape. However, it is noteworthy that these residual uncertainties do not violate the data consistency on the measurement space. Additionally, in Fourier phase retrieval, text guidance helps to effectively reconstruct consistently clean images by breaking inherent system symmetries, whereas the same algorithm without text guidance fails to consistently produce correct solutions (Figure 1). For more results, please refer to the Appendix.

Accuracy of obtained solution. To evaluate the quality of the obtained solution by TReg, we conduct a quantitative comparison with baseline methods for super-resolution and deblur tasks. The evaluation is based on three metrics: LPIPS, the mean squared error between the provided measurement and the

<i>SRx16</i>		Fired Rice \rightarrow Spaghetti			Ice Cream \rightarrow Macaron		
# stages	method	LPIPS \downarrow	CLIP-sim \uparrow	y-MSE \downarrow	LPIPS \downarrow	CLIP-sim \uparrow	y-MSE \downarrow
1	Ours	<u>0.769</u>	0.303	0.005	<u>0.771</u>	<u>0.314</u>	0.004
	PSLD	0.756	0.265	0.020	0.743	0.293	0.020
2	PnP	0.826	0.251	0.005	0.808	0.239	<u>0.005</u>
	PSLD+DDS	0.788	0.247	<u>0.010</u>	<u>0.772</u>	0.328	0.013
3	PSLD+PnP	0.801	<u>0.291</u>	0.014	0.784	0.306	0.008
<i>Deblur</i>		Fired Rice \rightarrow Spaghetti			Ice Cream \rightarrow Macaron		
# stages	method	LPIPS \downarrow	CLIP-sim \uparrow	y-MSE \downarrow	LPIPS \downarrow	CLIP-sim \uparrow	y-MSE \downarrow
1	Ours	0.737	<u>0.300</u>	0.013	0.743	<u>0.312</u>	0.011
	PSLD	0.798	0.274	0.013	0.750	0.252	0.011
2	PnP	0.798	0.259	0.015	0.752	0.248	0.011
	PSLD+DDS	0.768	0.247	<u>0.014</u>	0.752	0.300	0.015
3	PSLD+PnP	<u>0.761</u>	0.312	0.016	<u>0.751</u>	0.319	<u>0.013</u>

Table 1: Quantitative evaluation of SRx16 and Gaussian Deblurring task. Mean values are reported. **Bold:** the best score, underline: the second best.

predicted measurement, namely y-MSE⁴, and the CLIP similarity between the reconstructed image and the text prompt following the prior works in image editing [15, 36]. Each metric provides 1) quality of the reconstructed images, 2) data consistency, and 3) quality of text guidance, which allows us to investigate the advantage of TReg on inverse problems. Note that LPIPS is computed with respect to real images with the class of target prompt.

The results in Table 1 indicate that the solution obtained exhibits high quality while preserving data consistency, as evidenced by lower LPIPS and y-MSE values compared to the baselines. For some cases, PSLD achieves notably lower LPIPS but solutions are lost data consistency and exhibit large y-MSE values with significantly different reconstructions as shown in the fourth column of Figure 4. In the case of CLIP similarity, TReg is comparable or superior compared to state-of-the-art image editing algorithms, highlighting the efficacy of text-guidance facilitated by TReg. Direct application of the editing algorithm to the measurement, referred to as PnP, yields sub-optimal performance across all metrics. In the case of y-MSE, PnP achieves a lower value due to minimal alterations made to the measurement, as depicted in the last column of Figure 4. Also, the performance of sequential approaches shows that reconstruction error is accumulated at each stage, resulting in substantial errors in the final outcome. In contrast, TReg effectively integrates the given text prompt while preserving robust data consistency, thereby validating its efficacy.

Figure 4 presents a qualitative comparison between the proposed method and the baseline methods. The quality of the reconstructed image aligns with the quantitative results. Interestingly, PnP and DDS show a notable similarity in the direction of editing, with DDS tending to generate relatively sharper images. However, both methods compromise consistency with the given measurement.

⁴ In formula, we compute $\|\mathbf{y} - \mathcal{A}(\mathbf{x})\|_2^2$.

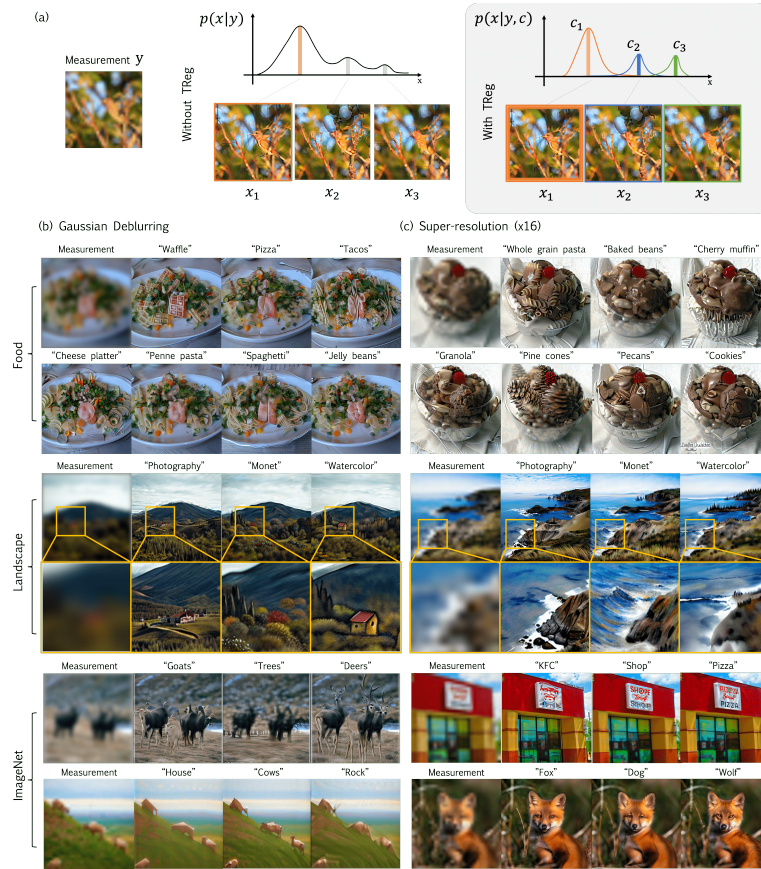


Fig. 5: Solving inverse problem with multiple prompts. Measurements are generated from ImageNet, Food101, and Landscape dataset. (a) With $TReg$, we can solve the inverse problem with multiple prompts for a fixed measurement. (b) Deblur (Gauss) (c) Super-resolution. Best views are displayed.

In contrast, our method effectively preserves data consistency. Meanwhile, we also compare the results of our method without $TReg$ and $PSLD$ with CFG guidance. When $TReg$ is removed from our method (third column in Figure 4), it provides a solution that aligns well with the given measurement but generates arbitrary structures. This result highlights the impact of $TReg$ that reduces the ambiguity of inverse problem solving. $PSLD$ with CFG guidance (fourth column in Figure 4) also fails to appropriately reflect given text prompt, as there is no consideration for text-guidance in solving inverse problems.

Furthermore, we conduct a qualitative comparison for box inpainting task, illustrated in Figure 6 (a), $TReg$ reconstructs image properly according to the given text prompt with higher fidelity compared to baseline methods. From Figure 6 (b), we repeatedly observe that text regularization enables the discovery of

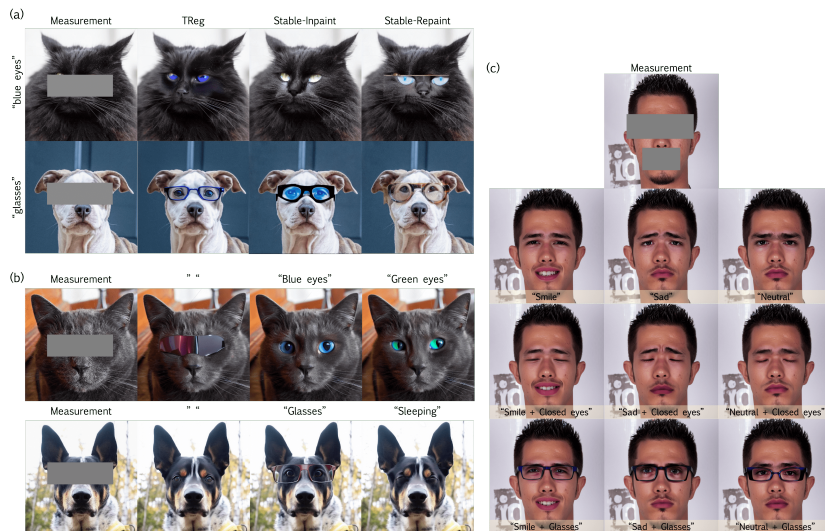


Fig. 6: Representative results for box inpainting task. (a) TReg is better at finding solution according to text with high-fidelity. (b) Text regularization helps to reconstruct as intended. (c) TReg is possible to reconstruct based on multiple concepts.

solutions as intended. It allows the discovery of even rare solutions, such as a cat with green eyes. Additionally, in Figure 6 (c), TReg demonstrates its capability to solve the inpainting problem by composing concepts. In other words, TReg can narrow down the solution space by utilizing not only a singular concept but also multiple concepts simultaneously.

4.3 Robustness of TReg with diverse texts and image domains

In previous sections, we demonstrate that TReg successfully mitigates the uncertainty of inverse problems and produces accurate reconstruction consistently. We further investigate the robustness of TReg with diverse set of texts and image domain such as landscape. Given that the primary role of TReg is to reduce the solution space according to $p(\mathbf{z}|\mathbf{c})$, the proposed method is expected to reconstruct diverse images in response to the provided text prompt. Figure 5 illustrates the results of solving inverse problems for super-resolution and deblur tasks with various text prompts. Regardless of the forward operation or data domain, TReg effectively reconstructs the solution. Importantly, different solutions maintain consistency with the given measurement. This distinctive feature sets our proposed approach apart from conventional stylization or personalization methods. Furthermore, the result directly shows the existence of multiple solutions that satisfied given forward model, which is an evidence of the ill-posedness nature of the inverse problem.

5 Related work

Leveraging text prompts for inverse problem solving has been studied in several recent works. TextIR [1] incorporates text embedding from CLIP during the training of an image restoration network to constrain the solution space in the case of extreme inverse problems. DA-CLIP [24] takes a similar approach of leveraging the embeddings and applies it to diffusion bridges. P2L [11] proposes to automatically tune text embedding on-the-fly while running a generic diffusion inverse problem solver. Notably, the latter two methods [11, 24] are focused on improving the overall performance rather than constraining the solution space. TextIR has similar objective to *TReg*, but requires task-specific training. In this regard, to the best of our knowledge, *TReg* is the first general diffusion-based inverse problem solver that does not require task-specific training, while being able to incorporate text conditions to effectively control the solution space in general inverse problems.

6 Conclusion

This study introduced a novel concept of latent diffusion inverse solver with *regularization by texts*, namely *TReg*. The proposed solver minimizes ambiguity in solving inverse problems, effectively reducing uncertainty and improving accuracy in visual reconstructions, bridging the gap between human perception and machine-based interpretation. To achieve this, we derived LDM-based reverse sampling steps to minimize data consistency with text-driven regularization, consisting of adaptive negation. Specifically, to effectively integrate textual cues and guide reverse sampling, the paper introduced a null text optimization approach. Experimental results and visualizations demonstrated that text-driven regularization effectively reduces the uncertainty of solving inverse problems, and further enables text-guided control of signal reconstruction.

7 Potential negative impacts

In this study, the proposed text regularization is heavily influenced by prior. Therefore, if there is bias in a model utilized as a prior, such as in the case of stable diffusion, the solution to the inverse problem may also contain bias. As a restoration model controllable through text, there is a potential for misuse, such as the generation of fake news. Countermeasures should be established to prevent incorrect results and ensure the integrity of the outcomes.

Supplementary material of "Regularization by Texts for Latent Diffusion Inverse Solvers"

Jeongsol Kim^{1,*}, Geon Yeong Park^{1,*}, Hyungjin Chung¹, and Jong Chul Ye²

¹ Dept. of Bio & Brain Engineering, KAIST

² Kim Jae Chul AI graduate school, KAIST

{jeongsol, pky3436, hj.chung, jong.ye}@kaist.ac.kr

* Equal contribution

1 Implementation Details

In this section, we provide further details on implementation of *TReg*. The code will be available to public on <https://github.com/TReg-inverse/Treg>.

1.1 Stable-diffusion and CLIP

We leverage the pre-trained Latent Diffusion Model (LDM), including an auto-encoder and the U-net model, provided by diffusers. Due to the limitation of its modularity, we implement the sampling process for inverse problems by ourselves, rather than changing given pipelines. The Stable-diffusion v1.5 is utilized for every experiment in this work, and the ViT-L/14 backbone and its checkpoint is used for CLIP image encoder for adaptive negation.

1.2 Conjugate gradient method

In this work, we apply the CG method to find a solution to the following problem:

$$\min_x \frac{\|\mathbf{y} - \mathcal{A}\mathbf{x}\|_2^2}{2\sigma^2} + \lambda \|\mathbf{x} - \mathcal{D}_\varphi(\hat{\mathbf{z}}_{0|t})\|_2^2. \quad (1)$$

As the objective function is a convex function, the solution \mathbf{x}^* should satisfy

$$-\mathcal{A}^\top(\mathbf{y} - \mathcal{A}\mathbf{x}^*) + \lambda(\mathbf{x}^* - \mathcal{D}_\varphi(\hat{\mathbf{z}}_{0|t})) = 0, \quad (2)$$

where the coefficients are absorbed to λ . Then, we can formulate it as a linear system as

$$(\lambda\mathbf{I} + \mathcal{A}^\top\mathcal{A})\mathbf{x}^* = \lambda\mathcal{D}_\varphi(\hat{\mathbf{z}}_{0|t}) + \mathcal{A}^\top\mathbf{y} \quad (3)$$

where $\mathbf{A} = \lambda\mathbf{I} + \mathcal{A}^\top\mathcal{A}$ and $\mathbf{b} = \lambda\mathcal{D}_\varphi(\hat{\mathbf{z}}_{0|t}) + \mathcal{A}^\top\mathbf{y}$. Thus, we can solve (3) by CG method. In this work, we use 5 iterations of CG update with $\lambda = 1e-4$ for each time step if not explicitly stated otherwise.

1.3 CG update range

The data consistency update with CG algorithms is applied for a subset of sampling steps as described by Γ in Algorithm 1 of the main paper. Our empirical observation show that this partial data consistency update achieves better trade-off between the image reconstruction consistency and the latent stability. In the absence of the data consistency update, we employ the deterministic DDIM sampling step by setting $\eta\tilde{\beta}_t = 0$ or apply DPS gradient to improve the reconstruction quality. Overall, for inverse problems except the Fourier phase retrieval, we set the Network Function Evaluation (NFE) to 200 and design $\Gamma = \{t|t \bmod 3 = 0, t \leq 850\}$ ³, where mod denotes the modulo operation. For the Fourier phase retrieval, we set $\Gamma = \{t|t \bmod 10 = 0\}$.

1.4 TReg with DPS update

In the main manuscript, we only describe the pseudocode of TReg without DPS update for the readability. However, the algorithm could readily conduct an additional DPS update as follow. Under the definition of stochastic noise to be added at each timestep,

$$\tilde{\epsilon}_t := \frac{\sqrt{1 - \bar{\alpha}_{t-1} - \eta^2 \tilde{\beta}_t^2} \hat{\epsilon}_\theta + \eta \tilde{\beta}_t \epsilon}{\sqrt{1 - \bar{\alpha}_{t-1}}} \quad (4)$$

the pseudocode could be described as in Algorithm 2. We have used this additional DPS step for the box inpainting and Fourier phase retrieval task with step size $\rho_t = \sqrt{\bar{\alpha}_{t-1}}$. For box inpainting task, we set CFG scale ω_2 for DPS gradient to 0, while we set CFG scale $\omega_2 = \omega_1$ in Fourier phase retrieval task.

1.5 CFG guidance scale

The classifier-free guidance (CFG) is defined as

$$\hat{\epsilon}_\theta = \epsilon_\theta(\mathbf{z}_t, \phi, t) + \omega(\epsilon_\theta(\mathbf{z}_t, \mathbf{c}, t) - \epsilon_\theta(\mathbf{z}_t, \phi, t)) \quad (5)$$

where ω is a scale for the guidance. In other words, ω could be interpreted as a magnitude for the negation. Thus, we leverage ω to control the extent of enhancement applied to a given text prompt. In fact, we can regulate the same feature by adjusting the null-text update strategy, including null-text update frequency and number of optimization iterations per time step. However, the CFG guidance scale is simpler and more intuitive than adjusting the null-text update strategy. Hence, we have used a proper CFG scale while fixing the null-text update schedule Γ .

For the main experiments with the Food101 dataset in the main paper, we use the default scale 7.5 for all results. For the Fourier phase retrieval

³ The pre-trained Stable-diffusion uses $T = 1000$. Thus, $t = 850$ is equivalent to the sampling step with $\text{NFE} = 170$.

Algorithm 2 Inverse problem solving with TReg with DPS

Require: $\epsilon_\theta, \emptyset, c, \mathcal{E}, \mathcal{D}, \mathcal{A}, y, \mathcal{T}_{img}$
 $\mathbf{z}_T \sim \mathcal{N}(0, \mathbf{I})$
for $t \in [T, 1]$ **do**
 if $t \in \Gamma$ **then**
 $\hat{\epsilon}_\theta^{\omega_1}(\mathbf{z}_t) = \epsilon_\theta(\mathbf{z}_t, \emptyset, t) + \omega_1(\epsilon_\theta(\mathbf{z}_t, \mathbf{c}, t) - \epsilon_\theta(\mathbf{z}_t, \emptyset, t))$
 $\hat{\mathbf{z}}_{0|t} = (\mathbf{z}_t - \sqrt{1 - \bar{\alpha}_t} \hat{\epsilon}_\theta^{\omega_1}(\mathbf{z}_t)) / \sqrt{\bar{\alpha}_t}$
 $\tilde{\epsilon}_t \leftarrow$ Compute noise using (4)
 $\hat{\mathbf{x}}_0 \leftarrow \mathcal{D}(\hat{\mathbf{z}}_{0|t})$
 $\hat{\mathbf{x}}_0(\mathbf{y}) \leftarrow \arg \min_{\mathbf{x}} \frac{\|\mathbf{y} - \mathcal{A}(\mathbf{x})\|_2^2}{2\sigma^2} + \lambda \|\mathbf{x} - \hat{\mathbf{x}}_0\|_2^2$
 $\hat{\mathbf{z}}_0(\mathbf{y}) \leftarrow \mathcal{E}(\hat{\mathbf{x}}_0(\mathbf{y}))$
 $\hat{\mathbf{z}}_0^{ema} \leftarrow \bar{\alpha}_{t-1} \hat{\mathbf{z}}_0(\mathbf{y}) + (1 - \bar{\alpha}_{t-1}) \hat{\mathbf{z}}_{0|t}$ ▷ Latent Optimization
 $\mathbf{z}_{t-1} \leftarrow \sqrt{\bar{\alpha}_{t-1}} \hat{\mathbf{z}}_0^{ema} + \sqrt{1 - \bar{\alpha}_{t-1}} \tilde{\epsilon}_t$
 $c_\emptyset \leftarrow c_\emptyset - \eta \nabla_{\theta} \text{sim}(\mathcal{T}_{img}(\hat{\mathbf{x}}_0(\mathbf{y})), c_\emptyset)$ ▷ Adaptive negation
 else
 $\hat{\epsilon}_\theta^{\omega_2}(\mathbf{z}_t) = \epsilon_\theta(\mathbf{z}_t, \emptyset, t) + \omega_2(\epsilon_\theta(\mathbf{z}_t, \mathbf{c}, t) - \epsilon_\theta(\mathbf{z}_t, \emptyset, t))$
 $\hat{\mathbf{z}}_{0|t} = (\mathbf{z}_t - \sqrt{1 - \bar{\alpha}_t} \hat{\epsilon}_\theta^{\omega_2}(\mathbf{z}_t)) / \sqrt{\bar{\alpha}_t}$
 $\tilde{\epsilon}_t \leftarrow$ Compute noise using (4)
 $\mathbf{z}'_{t-1} \leftarrow \sqrt{\bar{\alpha}_{t-1}} \hat{\mathbf{z}}_{0|t} + \sqrt{1 - \bar{\alpha}_{t-1}} \tilde{\epsilon}_t$
 $\mathbf{z}_{t-1} \leftarrow \mathbf{z}'_{t-1} - \rho_t \nabla_{\mathbf{z}_t} \|\mathcal{A}(\mathcal{D}_\varphi(\hat{\mathbf{z}}_{0|t})) - \mathbf{y}\|$
 end if
end for

problem, we set the CFG scale $\omega_1 = \omega_2 = 4.0$. For other results, CFG scale among $\{3.0, 4.0, 5.0, 7.5\}$ provide robust performance for various datasets including FFHQ, AFHQ, LHQ (landscape dataset), and ImageNet.

1.6 Optimization problem for Fourier phase retrieval

In contrast other inverse problems with linear operation, Fourier phase retrieval involves non-linear operation so we cannot leverage CG to solve the optimization problem in pixel space. Thus, we use Adam optimizer with learning rate $1e - 3$ and $\beta_1 = 0.9, \beta_2 = 0.999$ to obtain the solution of

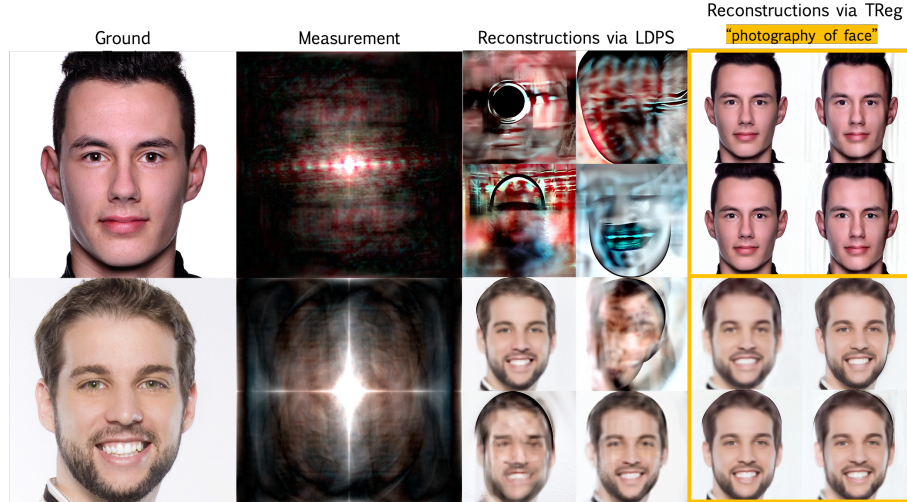
$$\min_{\mathbf{x}} \frac{\|\mathbf{y} - \mathcal{A}(\mathbf{x})\|_2^2}{2\sigma^2} + \lambda \|\mathbf{x} - \hat{\mathbf{x}}_0\|_2^2 \quad (6)$$

by setting $\lambda = 0$. This induces additional computational costs to solve the optimization problem. However, as analyzed in Section 2, these costs are comparable to those of other baseline algorithms, while consistently achieving the reconstruction of a unique solution.

2 Runtime Analysis

We propose text regularization by defining a proximal optimization problem in the latent space. While we introduce a two-step optimization problem-solving ap-

	PSLD	PSLD w/ AN	TReg
Linear	1.47	1.47	0.26
Non-linear	1.12	1.12	1.09

Table S1: Runtime (min) of each algorithm for NFE=200.**Fig. S1:** Additional results on Fourier Phase Retrieval. Best views are displayed.

proach, TReg does not require a large amount of computation time, as we leverage an accelerated optimization method, namely CG, and compute a closed-form solution for the subsequent problem. Consequently, TReg is effective compared to baseline algorithm, as shown in Table S1. We measure the runtime of linear inverse problem with delubbing task, and measure the runtime of non-linear inverse problem with Fourier phase retrieval task. Specifically, we did not use fixed point constraint of PSLD for the non-linear inverse problem as \mathcal{A}^T is not defined properly. Furthermore, the optimization variable for adaptive negation is only the text embedding, which does not incur a significant additional cost. Therefore, the runtime for adaptive negation is negligible (the second column of Table S1).

3 Additional Results

3.1 Fourier Phase Retrieval

In this section, we present additional examples for the Fourier phase retrieval problem. Specifically, we illustrate the variance of outcomes from the inverse problem solver without text regularization due to remaining symmetry, and

compare them with the consistent outcomes from the TReg, which breaks the symmetry. Figure S1 provides evidence for the capability of TReg to break the symmetry, contrasting with the LDPS algorithm without text regularization.

3.2 Super-resolution and Deblurring

In this section, we provide extended results for measurements to support the efficiency and compatibility of the proposed TReg with various domains. Specifically, we leverage the proposed method for super-resolution and delurring tasks on FFHQ. We examine the reconstruction with text prompts “baby face” and “adult face”. As shown in Figure S2, the proposed method successfully reconstructs images according to the given prompt, while the baseline method (sequential approach of PSLD and DDS) shows inferior reconstruction quality.



Fig. S2: Reconstruction result for SR (x16) and Deblur (Gaussian) task on FFHQ dataset. Our method outperforms the existing methods (PSLD+DDS) in terms of the reconstruction quality.

4 Limitation

While TReg demonstrates its performance in breaking the symmetry in the Fourier Phase Retrieval problem, its effectiveness is contingent upon the text prompt. For instance, when the true image features a complex or colorful background, a simple text prompt such as "a photography of a face" may not suffice to reconstruct a unique solution without residual symmetry.

In our scenario, we assume that the user can access the category of the dataset (e.g., FFHQ for faces). However, in real-world scenarios, it may be challenging to derive more informative text prompts solely from measurements with severe degradation. In general, finding suitable text prompts remains an open problem in text regularization for solving inverse problems.

References

1. Bai, Y., Wang, C., Xie, S., Dong, C., Yuan, C., Wang, Z.: Textir: A simple framework for text-based editable image restoration. arXiv preprint arXiv:2302.14736 (2023) [14](#)
2. Bond-Taylor, S., Willcocks, C.G.: ∞ -diff: Infinite resolution diffusion with subsampled mollified states. arXiv preprint arXiv:2303.18242 (2023) [4](#)
3. Bossard, L., Guillaumin, M., Van Gool, L.: Food-101 – mining discriminative components with random forests. In: European Conference on Computer Vision (2014) [8](#)
4. Boyd, S., Parikh, N., Chu, E., Peleato, B., Eckstein, J., et al.: Distributed optimization and statistical learning via the alternating direction method of multipliers. *Foundations and Trends® in Machine Learning* **3**(1), 1–122 (2011) [2](#), [5](#)
5. Choi, J., Kim, S., Jeong, Y., Gwon, Y., Yoon, S.: Ilvr: Conditioning method for denoising diffusion probabilistic models. arXiv preprint arXiv:2108.02938 (2021) [4](#)
6. Chung, H., Kim, J., Kim, S., Ye, J.C.: Parallel diffusion models of operator and image for blind inverse problems. In: Proceedings of the IEEE/CVF Conference on Computer Vision and Pattern Recognition. pp. 6059–6069 (2023) [4](#)
7. Chung, H., Kim, J., McCann, M.T., Klasky, M.L., Ye, J.C.: Diffusion posterior sampling for general noisy inverse problems. arXiv preprint arXiv:2209.14687 (2022) [2](#), [4](#), [7](#)
8. Chung, H., Lee, S., Ye, J.C.: Fast diffusion sampler for inverse problems by geometric decomposition. arXiv preprint arXiv:2303.05754 (2023) [4](#), [8](#)
9. Chung, H., Ryu, D., McCann, M.T., Klasky, M.L., Ye, J.C.: Solving 3d inverse problems using pre-trained 2d diffusion models. In: Proceedings of the IEEE/CVF Conference on Computer Vision and Pattern Recognition. pp. 22542–22551 (2023) [4](#)
10. Chung, H., Sim, B., Ye, J.C.: Come-closer-diffuse-faster: Accelerating conditional diffusion models for inverse problems through stochastic contraction. In: Proceedings of the IEEE/CVF Conference on Computer Vision and Pattern Recognition. pp. 12413–12422 (2022) [4](#)
11. Chung, H., Ye, J.C., Milanfar, P., Delbracio, M.: Prompt-tuning latent diffusion models for inverse problems. arXiv preprint arXiv:2310.01110 (2023) [14](#)
12. Deng, J., Dong, W., Socher, R., Li, L.J., Li, K., Fei-Fei, L.: Imagenet: A large-scale hierarchical image database. In: 2009 IEEE conference on computer vision and pattern recognition. pp. 248–255. Ieee (2009) [9](#)
13. Dhariwal, P., Nichol, A.: Diffusion models beat gans on image synthesis. *Advances in neural information processing systems* **34**, 8780–8794 (2021) [4](#)
14. He, L., Yan, H., Luo, M., Luo, K., Wang, W., Du, W., Chen, H., Yang, H., Zhang, Y.: Iterative reconstruction based on latent diffusion model for sparse data reconstruction. arXiv preprint arXiv:2307.12070 (2023) [4](#)
15. Hertz, A., Aberman, K., Cohen-Or, D.: Delta denoising score. In: Proceedings of the IEEE/CVF International Conference on Computer Vision. pp. 2328–2337 (2023) [8](#), [11](#)
16. Ho, J., Jain, A., Abbeel, P.: Denoising diffusion probabilistic models. *Advances in neural information processing systems* **33**, 6840–6851 (2020) [3](#)
17. Ho, J., Salimans, T.: Classifier-free diffusion guidance. arXiv preprint arXiv:2207.12598 (2022) [4](#), [5](#)
18. Kawar, B., Elad, M., Ermon, S., Song, J.: Denoising diffusion restoration models. *Advances in Neural Information Processing Systems* **35**, 23593–23606 (2022) [2](#), [4](#), [8](#)

19. Kingma, D.P., Welling, M.: Auto-encoding variational bayes. arXiv preprint arXiv:1312.6114 (2013) [3](#)
20. Lee, S., Chung, H., Park, M., Park, J., Ryu, W.S., Ye, J.C.: Improving 3d imaging with pre-trained perpendicular 2d diffusion models. arXiv preprint arXiv:2303.08440 (2023) [4](#)
21. Lester, B., Al-Rfou, R., Constant, N.: The power of scale for parameter-efficient prompt tuning. arXiv preprint arXiv:2104.08691 (2021) [5](#)
22. Loshchilov, I., Hutter, F.: Decoupled weight decay regularization. arXiv preprint arXiv:1711.05101 (2017) [9](#)
23. Lugmayr, A., Danelljan, M., Romero, A., Yu, F., Timofte, R., Van Gool, L.: Repaint: Inpainting using denoising diffusion probabilistic models. In: Proceedings of the IEEE/CVF Conference on Computer Vision and Pattern Recognition. pp. 11461–11471 (2022) [8](#)
24. Luo, Z., Gustafsson, F.K., Zhao, Z., Sjölund, J., Schön, T.B.: Controlling vision-language models for universal image restoration. arXiv preprint arXiv:2310.01018 (2023) [14](#)
25. Mardani, M., Song, J., Kautz, J., Vahdat, A.: A variational perspective on solving inverse problems with diffusion models. arXiv preprint arXiv:2305.04391 (2023) [2](#), [4](#)
26. Radford, A., Kim, J.W., Hallacy, C., Ramesh, A., Goh, G., Agarwal, S., Sastry, G., Askell, A., Mishkin, P., Clark, J., et al.: Learning transferable visual models from natural language supervision. In: International conference on machine learning. pp. 8748–8763. PMLR (2021) [5](#)
27. Romano, Y., Elad, M., Milanfar, P.: The little engine that could: Regularization by denoising (red). *SIAM Journal on Imaging Sciences* **10**(4), 1804–1844 (2017) [2](#)
28. Rombach, R., Blattmann, A., Lorenz, D., Esser, P., Ommer, B.: High-resolution image synthesis with latent diffusion models. In: Proceedings of the IEEE/CVF conference on computer vision and pattern recognition. pp. 10684–10695 (2022) [3](#)
29. Ronneberger, O., Fischer, P., Brox, T.: U-net: Convolutional networks for biomedical image segmentation. In: Medical Image Computing and Computer-Assisted Intervention—MICCAI 2015: 18th International Conference, Munich, Germany, October 5–9, 2015, Proceedings, Part III 18. pp. 234–241. Springer (2015) [3](#)
30. Rout, L., Raouf, N., Daras, G., Caramanis, C., Dimakis, A.G., Shakkottai, S.: Solving linear inverse problems provably via posterior sampling with latent diffusion models. arXiv preprint arXiv:2307.00619 (2023) [2](#), [4](#), [7](#), [8](#)
31. Sohl-Dickstein, J., Weiss, E., Maheswaranathan, N., Ganguli, S.: Deep unsupervised learning using nonequilibrium thermodynamics. In: International conference on machine learning. pp. 2256–2265. PMLR (2015) [3](#)
32. Song, B., Kwon, S.M., Zhang, Z., Hu, X., Qu, Q., Shen, L.: Solving inverse problems with latent diffusion models via hard data consistency. arXiv preprint arXiv:2307.08123 (2023) [4](#)
33. Song, J., Meng, C., Ermon, S.: Denoising diffusion implicit models. arXiv preprint arXiv:2010.02502 (2020) [3](#), [6](#)
34. Song, J., Vahdat, A., Mardani, M., Kautz, J.: Pseudoinverse-guided diffusion models for inverse problems. In: International Conference on Learning Representations (2022) [4](#), [8](#)
35. Song, Y., Sohl-Dickstein, J., Kingma, D.P., Kumar, A., Ermon, S., Poole, B.: Score-based generative modeling through stochastic differential equations. arXiv preprint arXiv:2011.13456 (2020) [3](#), [4](#)

36. Tumanyan, N., Geyer, M., Bagon, S., Dekel, T.: Plug-and-play diffusion features for text-driven image-to-image translation. In: Proceedings of the IEEE/CVF Conference on Computer Vision and Pattern Recognition. pp. 1921–1930 (2023) [8](#), [11](#)
37. Venkatakrisnan, S.V., Bouman, C.A., Wohlberg, B.: Plug-and-play priors for model based reconstruction. In: 2013 IEEE global conference on signal and information processing. pp. 945–948. IEEE (2013) [2](#)
38. Wang, Y., Yu, J., Zhang, J.: Zero-shot image restoration using denoising diffusion null-space model. arXiv preprint arXiv:2212.00490 (2022) [2](#), [4](#), [8](#)